Supplementary Information

Chasing Weakly Bound Biological Water Near Peptide Backbone in Aqueous Environment by Ultrafast 2D IR Infrared Spectroscopy

Table of Contents

1. Materials

N-ethylpropionamide (NEPA, 99% purity) was purchased from Sigma-Aldrich. It was lyophilized in deuterated water (D_2O) three times for the H/D exchange of the amide group, and then dissolved in D_2O at a concentration of 100 mM.

2. FTIR Spectroscopy

Infrared spectra were collected using Nicolet 6700 FTIR spectrometer equipped with a liquid nitrogen-cooled mercury-cadmium-telluride (MCT) detector. NEPA solution samples were placed in a home-made dual IR cell. The dual IR cell contained two 2-mm thick CaF_2 windows separated by a 30-μm thick "θ"-shaped Teflon spacer, which forms two independent sample compartments. The dual cell is made of copper, which is heated through a water bath for temperate-depended FTIR measurement. The NEPA/D_2O solution and pure liquid D_2O were placed in the two compartments separately. The dual cell was placed on a motorized translation stage so that the sample solution and solvent-only (background) spectra could be taken alternately. Dry air was used to purge FTIR spectrometer and the sample chamber during the IR spectral measurement. FTIR spectra were measured with a spectral resolution of 1 cm^{-1} and averaged by 64 scans from room temperature (23 °C) to 85 °C at 10°C interval.

3. Nonlinear IR Spectroscopy

2D quick shaper spectrometer (2D Quick, PhaseTech) was used to collect 2D IR spectra.[1-2] A typical laser pulse (3-mJ, sub 35-fs, 800-nm, 1000-Hz) was generated using a femtosecond laser system and was used to pump an optical parametric amplifier (OPA) to generate two near-IR pulses, i. e., the signal and idler pulses. The two near-IR pulses were further split by a dichroic mirror and independently controlled in time and collinearly aligned in space, and were loosely focused together on a nonlinear crystal ($AgGaS_2$) for difference-frequency generation (DFG), generating a 6-μJ mid-IR pulse centered at 6-μm with FWHM of ca. 270 cm^{-1}. The mid-IR pulse was split into pump and probe paths and then spatially and temporally overlapped in the sample. 2D IR signal was generated in the pump-probe geometry, and the polarization of the pump pulse was set as the same condition of the probe pulse. The pump pulse enters an IR pulse shaper (Ge-AOM) and generates a collinear pulse pair with modulated interval time (τ). The 2D-IR signal generated by the coincidence of the three pulses on the sample is in the direction of the probe pulse. The waiting time (T_w) between the pump and probe pulses is controlled by a pair of ZnSe wedges. Purely absorptive 2D-IR signal was detected and digitized using an IR monochromator equipped with a 64-element liquid nitrogen-cooled MCT array detector. The sample cell was packaged in the home-made temperature control component composed of a heating plate and a silicone rubber cover, both being connected to an intelligent temperature controller (ZNHW-III), which can maintain the temperature of the sample at a certain value during the 2D IR experiment. The temperature of the sample cell was measured by a PT100 temperature sensor. In this work, the nonlinear IR measurements were carried out at room temperature (about 23 °C), 50.0 °C, 60.0 °C, and 85.0 °C. Further, magic-angle IR pump-probe experiment was carried out at room temperature in order to evaluate the vibrational lifetime of the amide-I mode of NEPA in

D_2O.

4. Quantum Chemistry Calculations

Geometry optimization of NEPA and vibrational frequency analysis of its amide-I band, and those of NEPA–3(D_2O) clusters (Scheme 1), were carried out using the density functional theory (DFT) at the level of B3LYP/6-311++G (d, p). To simulate the second and weak hydrogen bond, the distance between the amide oxygen and the oxygen atom of the second water was fixed at 4.0 Å during the optimization. The energies of the *trans* NEPA and *cis* NEPA were obtained at the level of M062X/def2TZVP. All calculations were performed using Gaussian 09 program.[3]

5. Molecular Dynamics Simulations

MD simulations of NEPA in D_2O was performed using the NAMD program[4] with CHARMM force field[5] for NEPA. A SPC/E model was used for water. One NEPA molecule was solvated in a cubic solvent box with an initial size of 28 × 28 × 28 $Å^3$ containing 659 water molecules. The nonbonded cutoff distance was set to 12 Å, and the particle mesh Ewald summation was used for long-range electrostatic interaction. Before the MD simulations, the equilibration run was performed to ensure a stable NPT ensemble. The MD simulations were finally performed using the Langevin-piston Nose−Hoover method for 5 ns with a step of 20 fs using the NPT ensemble at normal atmospheric pressure and at 298 K.

In discussing the MD results, H and D are used interchangeably in this work.

6. NMR Spectroscopy

NMR sample was prepared by dissolving NEPA in H_2O at 200 mM concentration. One-dimensional ^1H and ^{13}C NMR spectra were measured using a 600 MHz Bruker Avance NMR spectrometer. The NMR results were shown in Supplementary Figure 2 and the chemical shifts were listed in Supplementary Table 1. Chemical shifts of H, H1, H2/H4, and H3 of *trans* NEPA are about 7.85, 3.13, 1.05 and 2.16 ppm respectively. The number ratio of four types of H agrees with the number of different H atoms in NEPA, indicating no *cis* amide conformation for NEPA. Chemical shifts of C, C1, C2, C3, and C4 are about 176.94, 34.03, 13.15, 28.76, and 9.24 ppm respectively. The lack of no extra chemical shifts for the same type of C atoms for the *cis* NEPA also provides no evidence for the assignment of *cis* amide conformation.

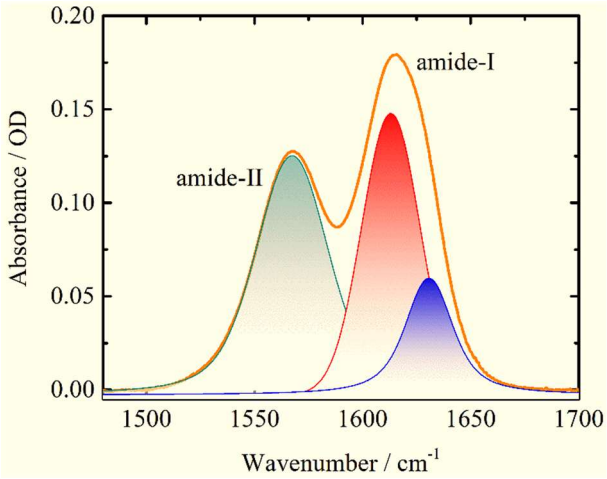

Supplementary Figure 1. FTIR spectrum of non-deuterated NEPA in H_2O obtained with 1 M concentration at 25 °C. The main amide-I peak of non-deuterated NEPA in H_2O locates at *ca*.1615.5 cm^{-1}. The infrared spectrum of the amide-I band can also be fitted by two Voigt functions, and the frequencies of the two subbands are 1613.1 and 1630.7 cm^{-1} (red filled and blue filled) respectively. The orange line is the experimental result. The green peak is the amide-II band, whose minor component on the low-frequency side is not considered in fitting.

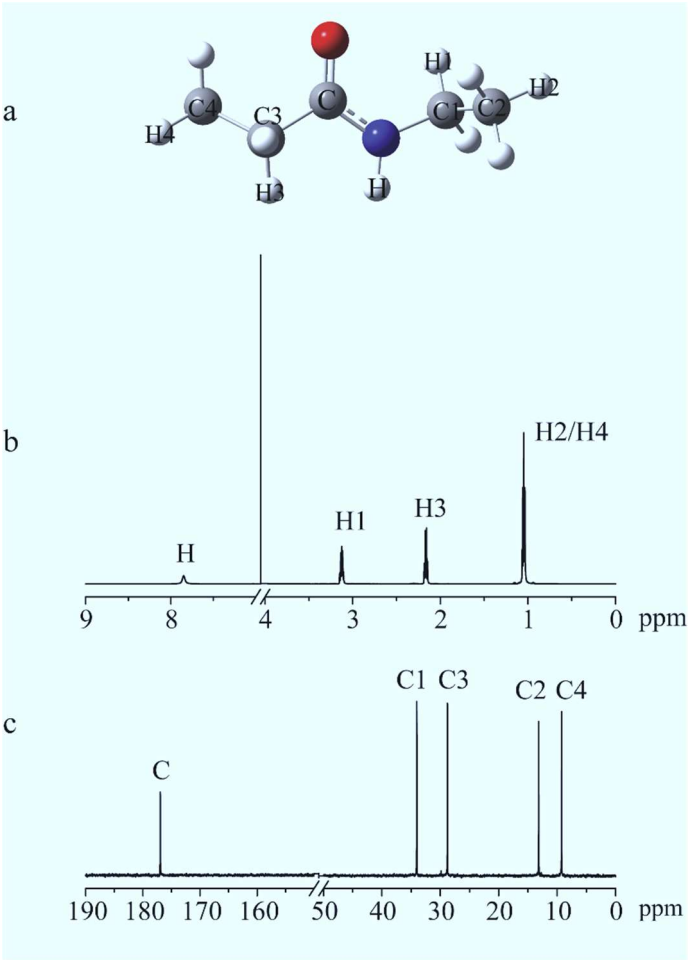

Supplementary Figure 2. Structure of NEPA (a) and 600-MHz ^{1}H (b) and ^{13}C (c) NMR spectra of NEPA in H_2O at 23 °C.

Supplementary Table 1. ^{1}H and ^{13}C Chemical Shifts (δ, in ppm) for NEPA in H_2O at 23 °C.

Atom type	δ	Atom type	δ
H	7.85	C	176.94
H1	3.13	C1	34.03
H2/H4	1.05	C2	13.15
H3	2.16	C3	28.76
		C4	9.24

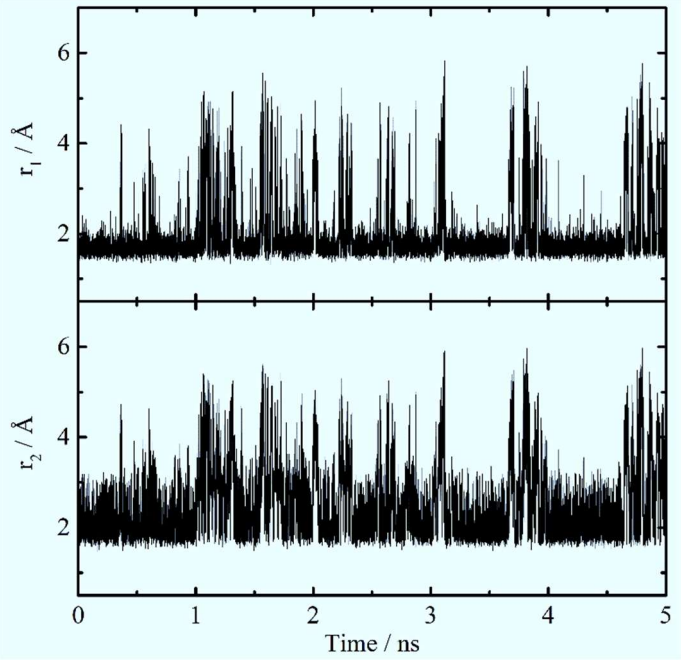

Supplementary Figure 3. Time evolutions of the nearest (r_1) and the second near (r_2) distances between the carbonyl oxygen of NEPA and the H atoms of water.

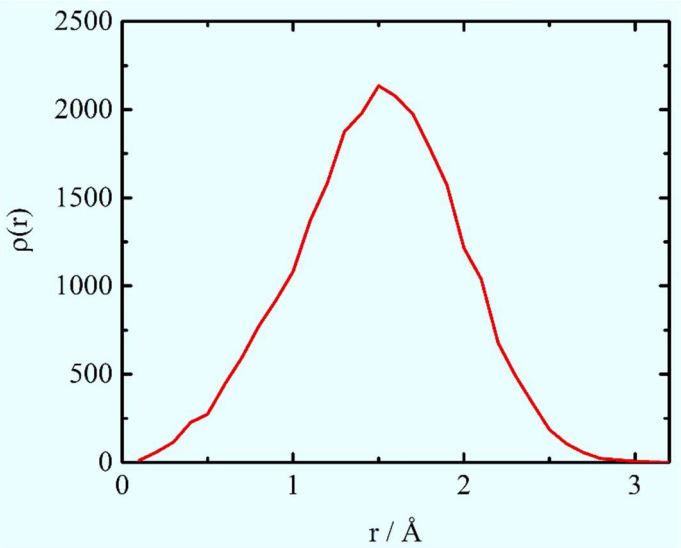

Supplementary Figure 4. Statistics of the nearest distance between the H atom of the NH group of NEPA and the O atom of water.

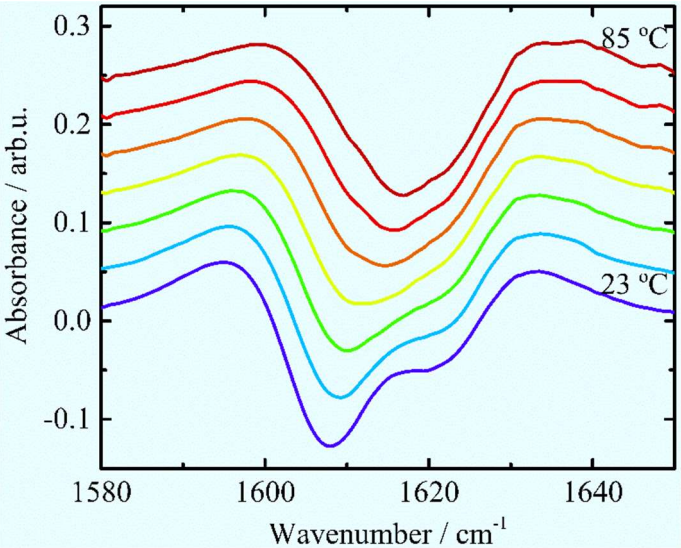

Supplementary Figure 5. Second-derivative FTIR spectra of NEPA in D_2O in the amide-I region as a function of temperature (23, 35, 45, 55, 65, 75, and 85 ℃).

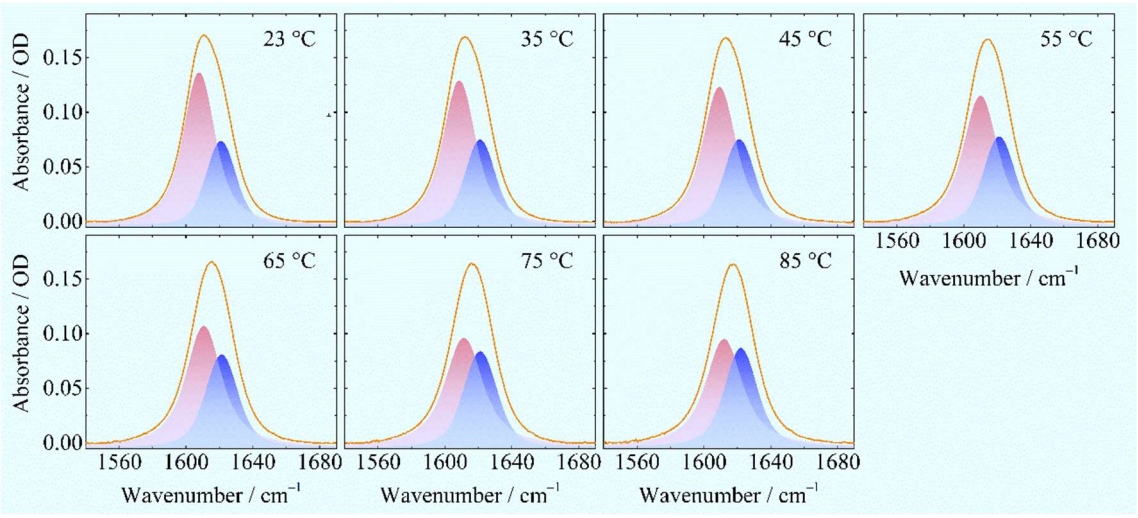

Supplementary Figure 6. Infrared spectra of the amide-I band of NEPA in D_2O as a function of temperature. The orange line in each panel is the experimental result. In each case, two shaded peaks are the fitting results using Voigt function.

Supplementary Table 2. Peak frequency (ω in cm^{-1}), relative peak areas and their ratio (A_{SHB}/A_{WHB}) of the two absorption components obtained by fitting the amide-I band of NEPA at different temperatures (T in °C). Equilibrium constant (K_{eq}) is computed at each temperature using Eq. (1).

T	ω_{SHB}	ω_{WHB}	A_{SHB}	A_{WHB}	A_{SHB}/A_{WHB}	K_{eq}
23	1607.85	1620.95	4.5156	2.0536	2.199	0.52141
35	1608.55	1621.04	4.4552	2.1816	2.042	0.56142
45	1609.25	1621.15	4.4341	2.2960	1.931	0.59368
55	1609.95	1621.19	4.3441	2.4043	1.807	0.63454
65	1610.65	1621. 36	4.2292	2.5370	1.667	0.68775
75	1611.35	1621.11	4.0534	2.6435	1.533	0.74770
85	1612.10	1622.23	4.0005	2.7565	1.451	0.78998

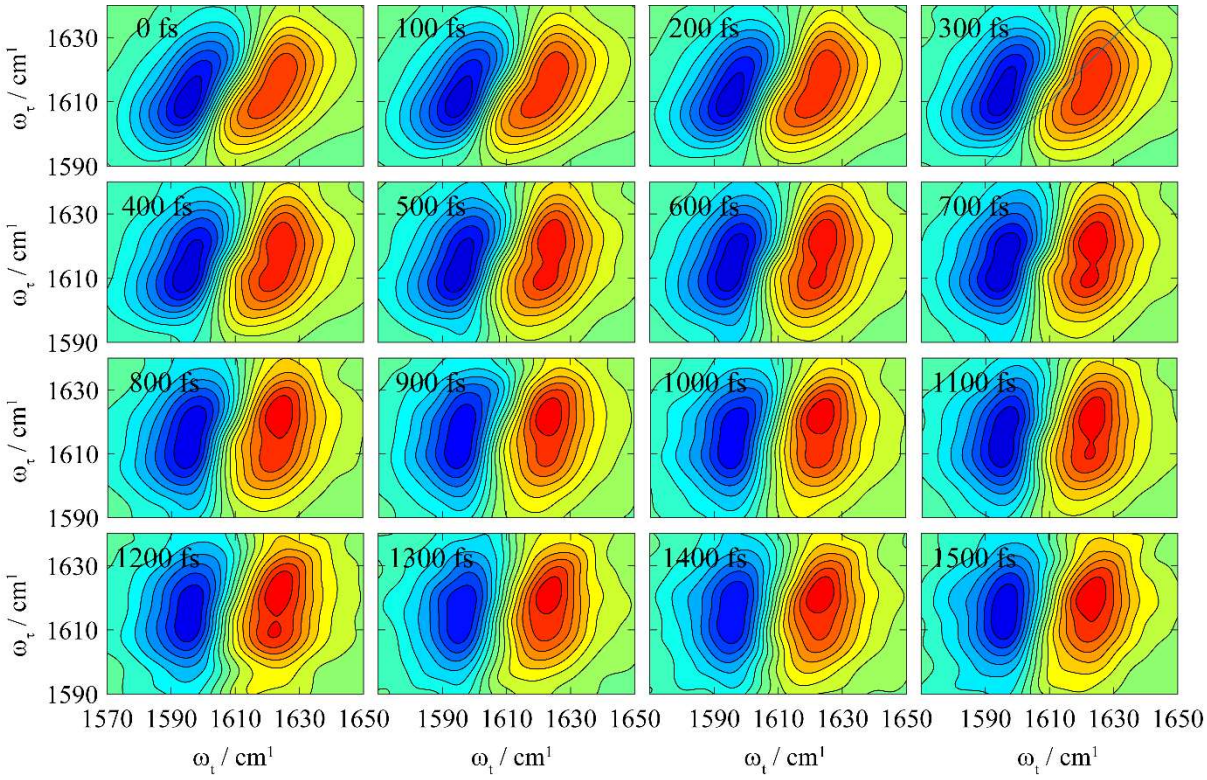

Supplementary Figure 7. Purely absorptive 2D IR spectra as a function of the waiting time at 23 °C.

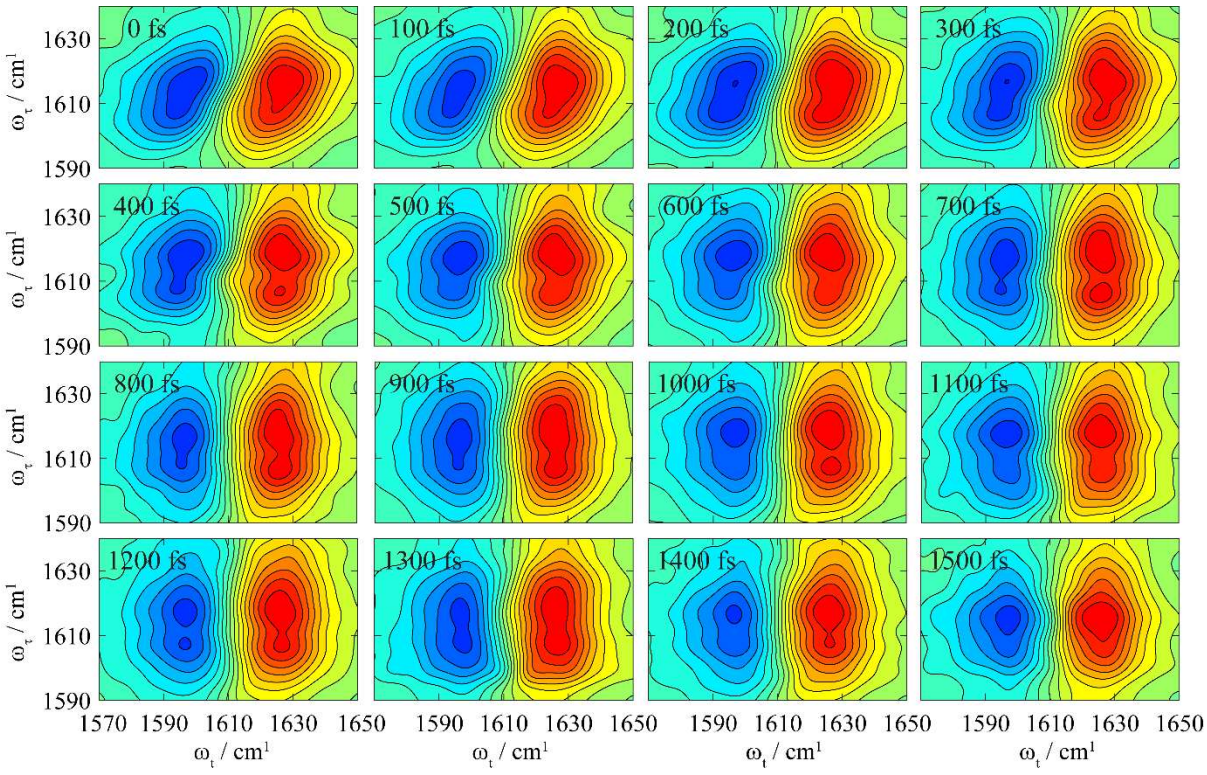

Supplementary Figure 9. Purely absorptive 2D IR spectra as a function of the waiting time

at 50 °C.

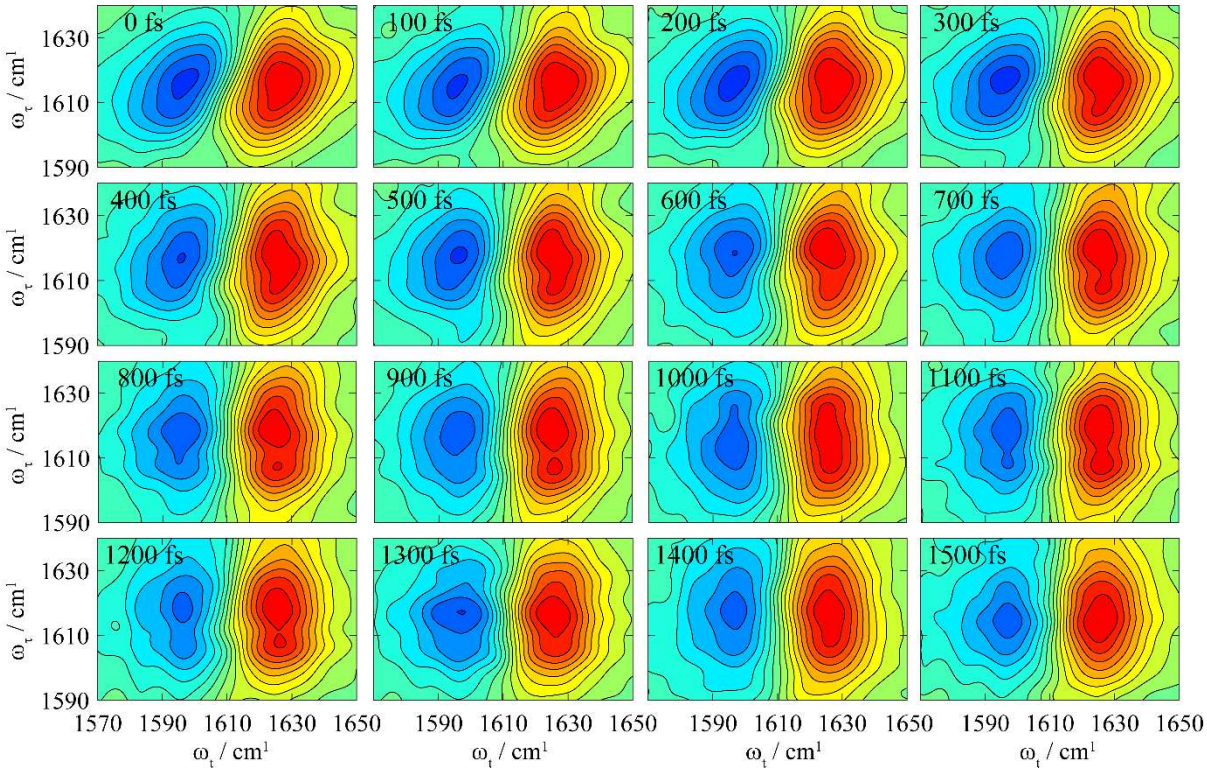

Supplementary Figure 8. Purely absorptive 2D IR spectra as a function of the waiting time at 60 °C.

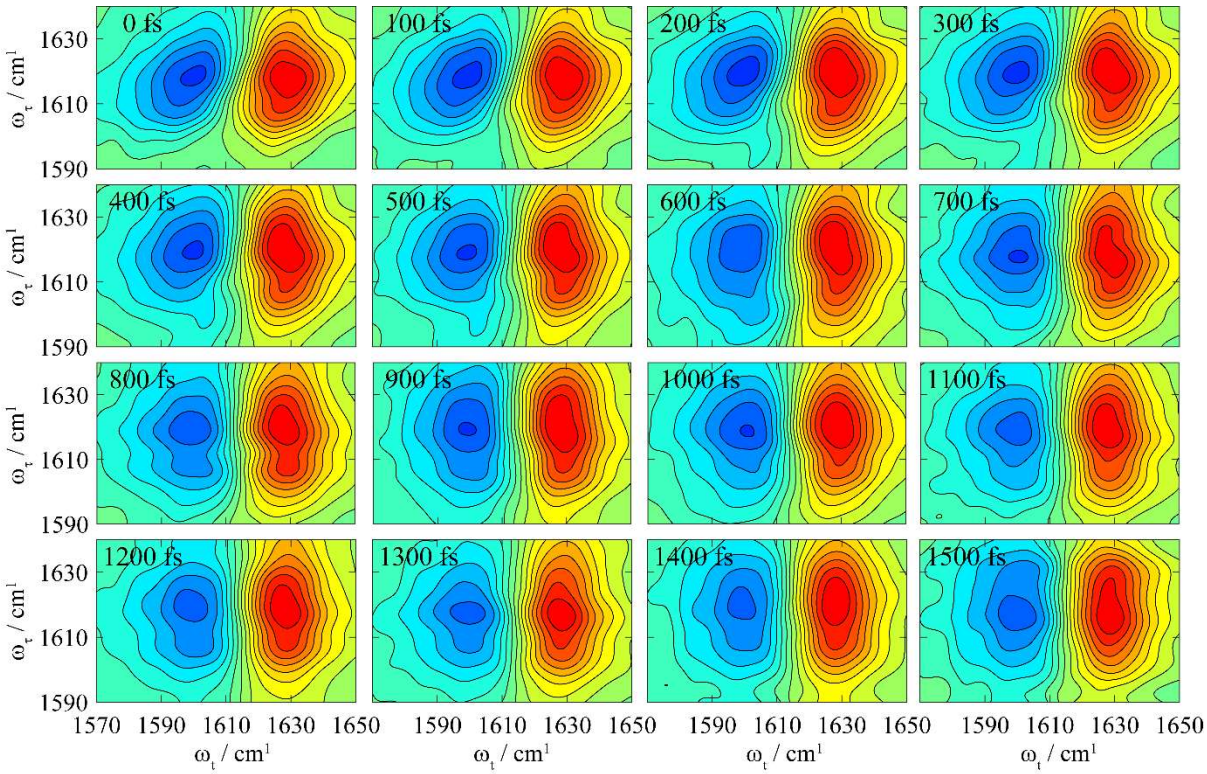

Supplementary Figure 10. Purely absorptive 2D IR spectra as a function of the waiting time at 85 °C.

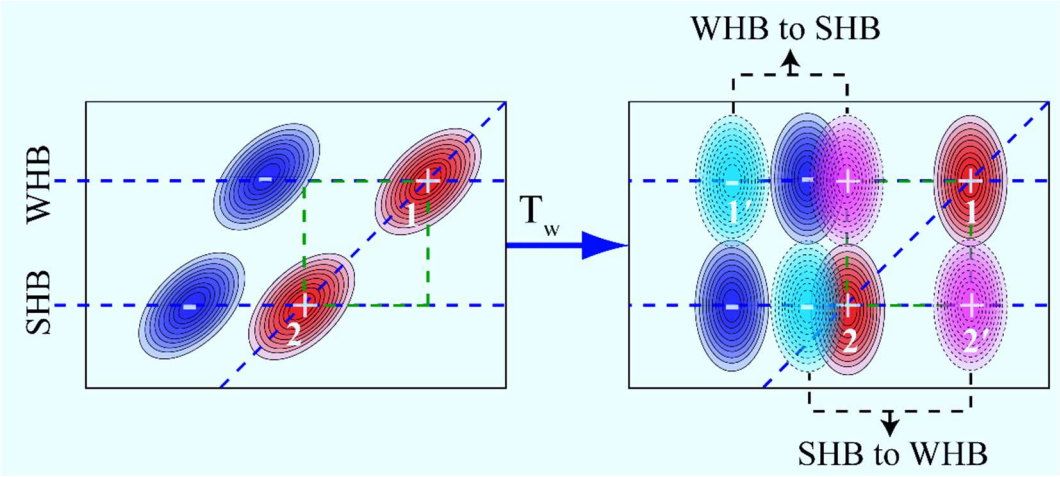

Supplementary Figure 11. An illustration of a typical 2D IR spectrum of the amide-I mode of NEPA at the initial moment and longer waiting time in the presence of chemical exchange. A pair of diagonal peaks (peak 1 for the 0-1 transition, i.e., from v = 0 to v =1, which is a positive signal; peak 1′ for the corresponding 1-2 transition, which is a negative signal) is the high-frequency component (weakly-hydrogen bonded amide, WHB), and another pair of diagonal peaks (peak 2 for the 0-1 transition and peak 2′ for the corresponding 1-2 transition) is the low-frequency component (strongly-hydrogen bonded amide, SHB). Chemical exchange from component 1 to 2 yields a pair of cross peaks in the upper left region, whereas that from component 2 to 1 yields a pair of cross peaks in the lower right region. Spectral overlap between positive and negative signals occurs so that the apparent intensity of peak 2 (and that of peak 1′) is affected.

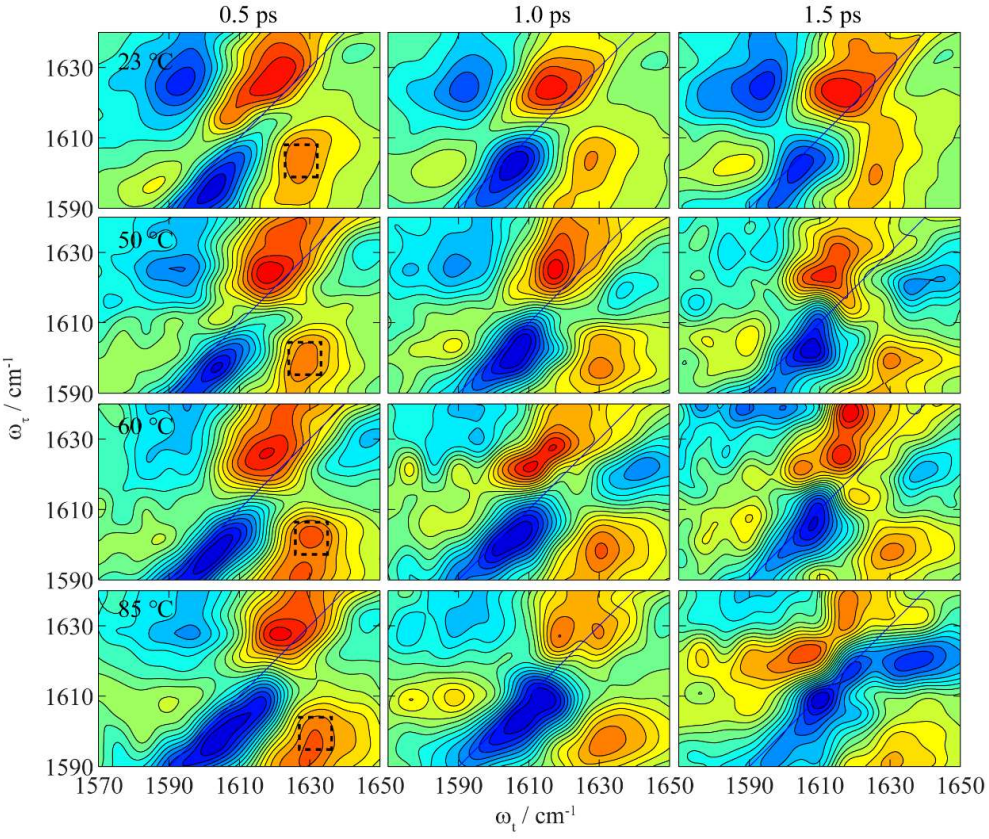

Supplementary Figure 12. Off-diagonal spectral components at three typical waiting times obtained by subtracting the 2D spectrum at T = 0 ps from those at varying waiting times, with dashed squares at 0.5 ps showing the integrated off-diagonal peak area (23 ℃: ω_τ = 1600.5 - 1605.4 cm^{-1} and ω_t = 1624.7 - 1629.7 cm^{-1}; 50 ℃: ω_τ = 1598.5 - 1603.4 cm^{-1} and ω_t = 1626.9 - 1631.9 cm^{-1}; 60 ℃: ω_τ = 1598.5 - 1603.4 cm^{-1} and ω_t = 1628 - 1633 cm^{-1}; 85 ℃: ω_τ = 1595.2 - 1600.1 cm^{-1} and ω_t = 1628.5 - 1633.5 cm^{-1}).

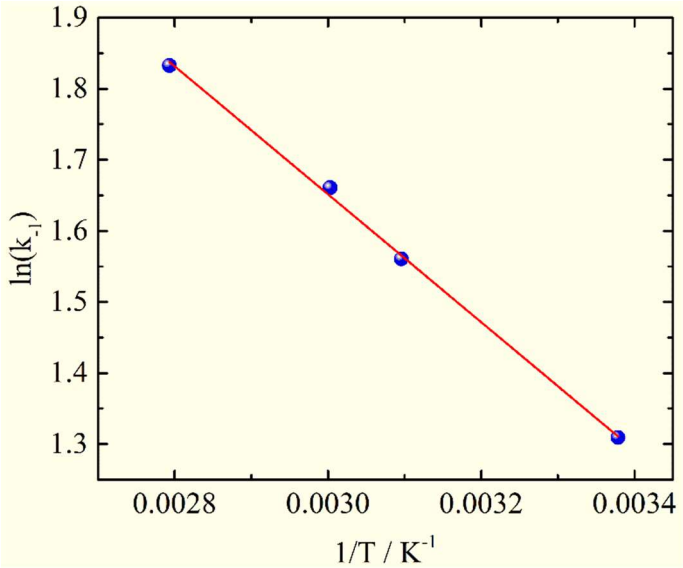

Supplementary Figure 13. Arrhenius plot of the rate constants k_{-1} for the change from the WHB state to the SHB state versus temperature and its fitting (red).

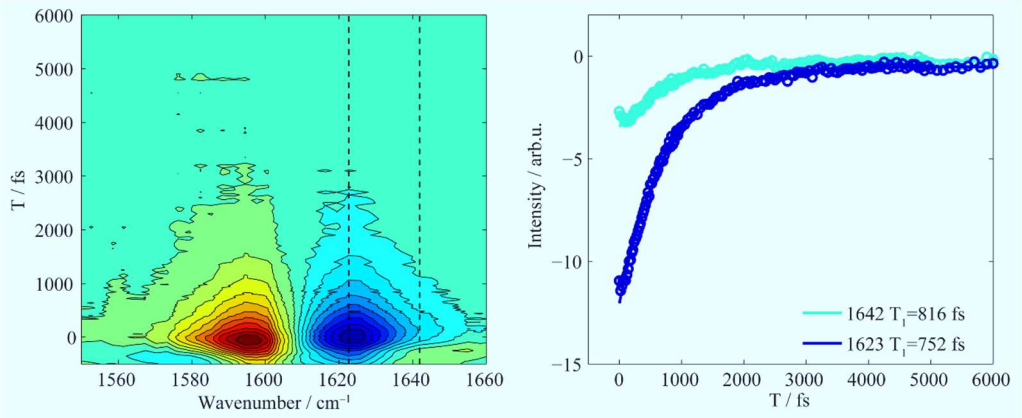

Supplementary Figure 14. Magic-angle IR pump probe spectra at 23 ℃ (left) and the vibrational relaxation dynamics traces extracted from the spectra (right) as a function of pump-probe delay time. This provides a good estimation of the T_1 time of the WHB and SHB states of the amide-I mode of NEPA in D_2O.

7. References

1. He, X.; Xu, F.; Yu, P.; Wu, Y.; Wang, F.; Zhao, Y.; Wang, J., Solvent-Dependent Structural Dynamics of an Azido-Platinum Complex Revealed by Linear and Nonlinear Infrared Spectroscopy. *Phys. Chem. Chem. Phys.* **2018,** *20*, 9984-9996.

2. Middleton, C. T.; Woys, A. M.; Mukherjee, S. S.; Zanni, M. T., Residue-Specific Structural Kinetics of Proteins through the Union of Isotope Labeling, Mid-IR Pulse Shaping, and Coherent 2D IR Spectroscopy. *Methods* **2010,** *52*, 12-22.
3. Frisch, M. J.; Trucks, G. W.; Schlegel, H. B.; Scuseria, G. E.; Robb, M. A.; Cheeseman, J. R.; Scalmani, G.; Barone, V.; Mennucci, B.; Petersson, G. A.; Nakatsuji, H.; Caricato, M.; Li, X.; Hratchian, H. P.; Izmaylov, A. F.; Bloino, J.; Zheng, G.; Sonnenberg, J. L.; Hada, M.; Ehara, M.; Toyota, K.; Fukuda, R.; Hasegawa, J.; Ishida, M.; Nakajima, T.; Honda, Y.; Kitao, O.; Nakai, H.; Vreven, T.; Montgomery, J. A.; Jr.; Peralta, J. E.; Ogliaro, F.; Bearpark, M.; Heyd, J. J.; Brothers, E.; Kudin, K. N.; Staroverov, V. N.; Kobayashi, R.; Normand, J.; Raghavachari, K.; Rendell, A.; Burant, J. C.; Iyengar, S. S.; Tomasi, J.; Cossi, M.; Rega, N.; Millam, J. M.; Klene, M.; Knox, J. E.; Cross, J. B.; Bakken, V.; Adamo, C.; Jaramillo, J.; Gomperts, R.; Stratmann, R. E.; Yazyev, O.; Austin, A. J.; Cammi, R.; Pomelli, C.; Ochterski, J. W.; Martin, R. L.; Morokuma, K.; Zakrzewski, V. G.; Voth, G. A.; Salvador, P.; Dannenberg, J. J.; Dapprich, S.; Daniels, A. D.; Farkas, O.; Foresman, J. B.; Ortiz, J. V.; Cioslowski, J.; Fox, D. J., *Gaussian 09, Revision A.02,*. Gaussian, Inc., Pittsburgh PA, 2009.
4. Phillips, J. C.; Braun, R.; Wang, W.; Gumbart, J.; Tajkhorshid, E.; Villa, E.; Chipot, C.; Skeel, R. D.; Kalé, L.; Schulten, K., Scalable Molecular Dynamics with NAMD. *J. Comput. Chem.* **2005,** *26*, 1781-1802.
5. MacKerell, A. D.; Bashford, D.; Bellott; Dunbrack, R. L.; Evanseck, J. D.; Field, M. J.; Fischer, S.; Gao, J.; Guo, H.; Ha, S.; Joseph-McCarthy, D.; Kuchnir, L.; Kuczera, K.; Lau, F. T. K.; Mattos, C.; Michnick, S.; Ngo, T.; Nguyen, D. T.; Prodhom, B.; Reiher, W. E.; Roux, B.; Schlenkrich, M.; Smith, J. C.; Stote, R.; Straub, J.; Watanabe, M.; Wiórkiewicz-Kuczera, J.; Yin, D.; Karplus, M., All-Atom Empirical Potential for Molecular Modeling and Dynamics Studies of Proteins. *J. Phys. Chem. B* **1998,** *102*, 3586-3616.